JOURNAL OF GEOPHYSICAL RESEARCH, VOL. 106, NO. A8, PAGES 15,929-15,940, AUGUST 1, 2001

Evolution of magnetic field fluctuations in high-speed solar wind streams: Ulysses and Helios observations

T. S. Horbury[1]
Astronomy Unit, Queen Mary and Westfield College, London

A. Balogh
The Blackett Laboratory, Imperial College, London

Abstract. Ulysses magnetic field measurements in high-speed streams emanating from the Sun's polar coronal holes reveal a complex combination of fluctuations on different scales. Measurements of the wavenumber dependence of radial and latitudinal power scaling, spectral index, and anisotropy of undisturbed polar magnetic field fluctuations between 1.4 and 4.1 astronomical units (AU) are presented. These results confirm earlier work and reveal the presence of three populations: structures at large scales, Alfvén waves at intermediate scales, and turbulent fluctuations at the smallest scales. A significant decrease in power with latitude, as a result of overexpansion of polar coronal holes, has consequences for energetic particle diffusion coefficients. Other results, in particular those related to field magnitude variations, are not well understood at this time. A similar analysis of magnetic field fluctuations in high-speed streams at low heliolatitudes between 0.3 and 1 AU, measured by the Helios spacecraft, shows consistency with Ulysses measurements, suggesting a common origin for fluctuations in all high-speed streams.

1. Introduction

Ulysses observations of the polar heliosphere near solar minimum have revealed the presence of relatively steady, high-speed (700-800 km s^{-1}) solar wind flows above around 40° heliolatitude [*Phillips et al.,* 1995a] which originate in the Sun's polar coronal holes. The nearly constant wind speed over all longitudes and a wide range of latitudes results in a lack of large-scale stream structure, such as corotating interaction regions (CIRs) and rarefaction regions [*Phillips et al.,* 1995a; *Balogh et al.,* 1995; *Forsyth et al.,* 1996a]. Therefore fluctuations within high-speed polar solar wind flows experience a considerably more homogeneous environment than those at low latitudes, making the polar heliosphere a useful region in which to study the behavior of magnetohydrodynamic (MHD) fluctuations undisturbed by stream structure. Indeed, since the solar wind is, as a high Reynolds' number and magnetic Reynolds' number collisionless plasma, the most accessible medium in which to study collisionless MHD turbulence, so the high-speed polar solar wind is the best region in which to study MHD fluctuations and turbulence relatively undisturbed by large-scale inhomogeneities. It is the high-speed solar wind at high latitudes, often termed the "polar solar wind," and specifically, the magnetic field fluctuations within it that are the subject of this paper.

In addition to the importance of polar fluctuations as examples of MHD turbulence, their behavior is pivotal in the transport of cosmic rays in the polar heliosphere (see, for example, *Potgieter* [1998] for a recent review). Estimates of power levels and spectral indices throughout the polar heliosphere are therefore important for the development of this still incompletely understood topic.

2. MHD Fluctuations in the Solar Wind

While many details remain unclear, the bulk properties of MHD scale fluctuations in the heliosphere have been well established, notably using Helios data between 0.3 and 1 astronomical units (AU) and Pioneer and Voyager data beyond 1 AU: See *Tu and Marsch* [1995], *Goldstein and Roberts* [1995], and *Matthaeus et al.* [1995] for comprehensive reviews. Fluctuations in high-speed (V_{SW} > ~600 km s^{-1}) and slow speed (V_{SW} < ~500 km s^{-1}) streams are rather different.

In high-speed streams, power levels are generally high (typically, $\delta B/|B| \sim 1$) with high levels of the normalized cross helicity σ_C, indicating the dominance of outward propagating Alfvénic fluctuations on a wide range of scales [e.g. *Marsch and Tu,* 1990]. Power in the field magnitude variations is typically an order of magnitude lower than that in the components, as a result of the low level of compressive (fast and slow mode) fluctuations.

It is possible to identify three distinct ranges of scales in MHD fluctuations in fast wind, on the basis of variations in the spectral index a of the field components: a high-frequency turbulent inertial range, where $\alpha \sim -5/3$ (the familiar Kolmogorov value); a low-frequency range, where $\alpha \sim -1$; and a transition regime between the two. The extension of the inertial and transition regimes to lower frequency with increasing solar distance [*Bavassano et al.,* 1982b] is an indication of energy transfer from the large-scale $1/f$ regime into an active turbulent cascade.

The low-frequency $1/f$ regime is, then, the source of power for the turbulent cascade: See, for example, *Tu et al.* [1984] for a discussion. These fluctuations are generated in the solar corona

[1]Now at The Blackett Laboratory, Imperial College, London.

Paper number 2000JA000108.
0148-0227/01/2000JA000108$09.00

(see, e.g., *Matthaeus and Goldstein* [1986] for a possible generation mechanism) and propagate outward essentially unchanged until they decay and transfer energy into the cascade. The WKB approximation [e.g., *Bazer and Hurley,* 1963] should apply to such waves, whose wavelengths are much shorter than the scale over which the solar wind bulk parameters vary. In this case, power levels should decrease with distance as $P(r) \propto r^{-3}$. Clearly, at higher frequencies within the turbulent cascade, where energy is being transferred to ever smaller scales, power should decrease more rapidly with distance than the WKB value.

The presence of large-scale stream structure at low latitudes makes the measurement of such power decreases rather difficult. In addition to the increase in power produced by compressions and shocks the collisions of fast and slow wind streams have the effect of slowing the fastest wind. These interactions also reduce the extent of high-speed solar wind streams with distance, making it harder to identify high-speed streams lasting several days at 1 AU than it is at 0.3 AU. Careful studies of radial power trends in high-speed wind, however, have generally revealed a faster than WKB decrease although *Marsch and Tu* [1990] showed that on relatively large scales, power decreases as r^{-3}, consistent with WKB. A careful study by *Roberts* [1989] also showed that on scales with wavenumbers around 10^{-7} - 10^{-6} km^{-1}, radial variations were consistent with WKB scaling. It is, of course, waves on these large scales, which have yet to decay and lose energy and are therefore not interacting with their environment, which should obey WKB scaling.

While there are structures, particularly those that are pressure balanced, present in the solar wind at essentially all scales [e.g., *Marsch and Tu,* 1993], at the largest scales there is a transition from turbulence and waves to structures being the dominant contributors to power levels. On the scale of days, because of the Sun's rotation, spacecraft pass from one solar wind stream to another. However, *Jokipii and Kóta* [1989] argued that field line movements due to supergranular motion would also be carried into the heliosphere. While such variations, with a typical spacecraft timescale of around 1 day at 1 AU, should be masked by stream-stream interactions at low latitudes, Jokipii and Kóta argued that in the polar heliosphere near solar minimum, with only high-speed wind over a wide range of latitudes, such variations could persist. In particular, since such variations should scale with distance as r^2, they can come to dominate higher-frequency fluctuations which obey WKB scaling. At low latitudes the presence of stream structure on scales above a day makes it impossible to study this behavior, although power decreases less rapidly than the WKB prediction [e.g., *Roberts et al.,* 1990], as a result of energy input from stream-stream interactions. It has been argued [e.g., *Roberts et al.,* 1987] that stream shear is also a strong driver of the turbulent cascade at low latitudes, at large scales.

In slow streams, power levels, like the bulk field and plasma properties, tend to be highly variable, but the spectral index α is typically near -5/3 over all MHD scales. As such, fluctuations in slow streams appear to be close to fully developed turbulence. The development of the turbulence cascade within high-speed wind is of interest in this work, and therefore slow-speed wind streams have been excluded from the data wherever possible.

The passage of Ulysses over the Sun's poles in 1994-1996 provided a wealth of data about the polar heliosphere near solar minimum. In particular, the lack of large-scale stream shear allows MHD fluctuations to propagate largely undisturbed out to very large distances. In addition, the polar heliosphere is important in controlling energetic particle propagation throughout the solar system, and magnetic field fluctuations act to scatter such particles, making the polar heliosphere an important region of study.

Early analysis revealed a similar population of fluctuations to those at low latitudes in high-speed streams: highly Alfvénic [*Goldstein et al.,* 1995], with a spectral index near -1 at low frequencies and -5/3 at high frequencies [*Horbury et al.,* 1996]. The extension of the turbulent regime to lower frequencies with increasing distance, again as seen at low latitudes, confirmed the presence of an active turbulent cascade [*Horbury et al.,* 1996].

Forsyth et al. [1996b] showed that polar power levels on hourly scales decreased faster than WKB, although *Jokipii et al.* [1995] showed that at larger scales the decrease was near r^{-2}, consistent with the predictions of *Jokipii and Kóta* [1989].

The aim of this paper is to provide, for the first time, estimates of the power scaling of fluctuations in the polar heliosphere over a wide range of scales. A fully self-consistent estimate of both latitude and distance dependence of magnetic field fluctuations, including those of the field magnitude, is presented, along with similar trends in spectral indices. In addition, a similar analysis of Helios data from high-speed streams between 0.3 and 1 AU provides a comparison with low-latitude fluctuations.

3. Analysis Method

The Ulysses spacecraft spent around 3 years within high-speed solar wind from the Sun's polar coronal holes, during southern and northern polar passes. Part of the orbit of the spacecraft is shown in Figure 1, with these two long periods within high-speed wind shown as bold lines. These periods were used in the analysis presented in this work. Corotating interaction regions (CIRs) extended to higher latitudes during the southern polar pass than during the northern, allowing observations in undisturbed high-speed wind at larger distances and lower latitudes during the northern pass. As a consequence, it is easier to discriminate

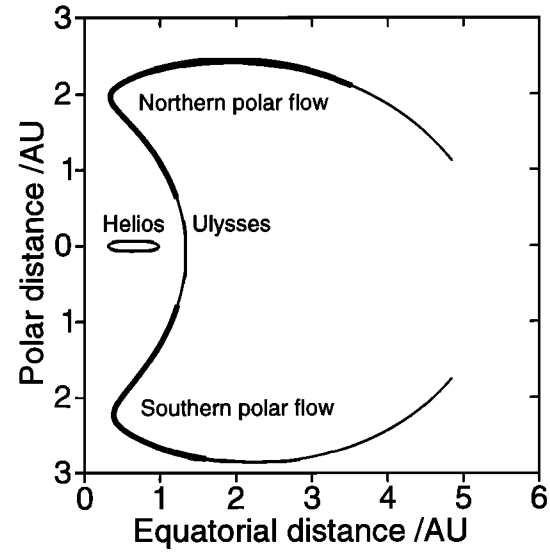

Figure 1. Comparison of the orbits of Ulysses and Helios 1. Orbits are despun relative to the Sun, showing solar distance in the solar equatorial and polar directions. This projection is a true representation of solar latitudes and distances. Only part of the Ulysses orbit is shown, from the middle of 1992 until late 1996. Parts of the Ulysses orbit when the spacecraft remained in high-speed polar flows for long periods are shown as thicker lines: These are the intervals analyzed in this work.

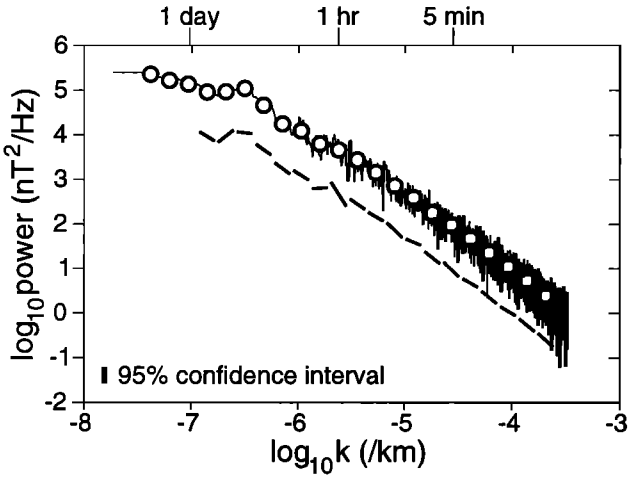

Figure 2. A typical power spectrum calculated from 5 days of 12-s-averaged Ulysses magnetic field data in high-speed polar solar wind. Data shown are for the *N* component. Open circles are power estimates in wavenumber ranges. It is these estimates that are used in the analysis in this work. Spectral index estimates are shown as lines displaced downward by a factor of 10.

latitude and distance effects from northern pass data and we concentrate on the northern pass in this work. The southern pass interval extends from day 110, 1994 (3.2 AU, 60°S), past peak latitude (day 257, 1994: 2.3 AU, 80°S) to day 15, 1995 (1.5 AU, 36°S). The northern interval extends from day 100, 1995 (1.4 AU, 28°N) past peak latitude (day 212, 1995: 2.0 AU, 80°N) to day 200, 1996 (4.1 AU, 31°N).

The Ulysses magnetic field experiment [*Balogh et al.*, 1992] returns one or two vector measurements of the in situ magnetic field every second, depending on data rate. To ensure an equally spaced data record and to eliminate dissipation scales and spacecraft effects, 12 s boxcar averages of the field were used. Data gaps are rare and tend to be small, usually when a data rate change occurs. Such data gaps, which typically comprise ~2% of the time during polar passes, were linearly interpolated in each field component and the field magnitude. The RTN coordinate system is used for Ulysses data throughout this work, where *R* points radially away from the Sun, *T* is the cross product of the Sun's rotation vector and *R*, and *N* makes up the right-handed set.

In order to study the radial and latitudinal variations of fluctuations in the high-speed solar wind at high latitudes, fluctuations in successive short intervals of data were analyzed. By considering changes between intervals as Ulysses moved in distance and latitude it is possible to separate variations in these directions. To allow the study of sufficiently large-scale variations in the magnetic field, 5 day intervals of data were studied. For each interval, magnetic field data for the *R*, *T*, and *N* components and the field magnitude were treated as separate data sets. Each set, after data gap filling (intervals with more than 5% data gaps were rejected), had a mean level removed. An estimate of the power spectral density of the data set was then made using a multitaper spectral estimator. Multitapering is discussed in detail by *Percival and Walden* [1993], so we provide only a brief description of the method here.

Two important problems associated with spectral estimation are those of leakage and confidence limits. Leakage of power between scales is particularly important for spectra with large dynamic ranges, such as turbulent signals. In this case, estimation of the spectral index is physically important but can be altered by leakage. In general, data tapering or prewhitening can alleviate these problems. However, conventional data tapers (such as Hamming or Hanning windows) artificially bias parts of the time series compared to others. Multiple overlapping taper (so-called weighted overlapped segment average or WOSA) methods are better but, again, alter the statistical weight of subsets of the data and additionally reduce spectral resolution of the estimate. Prewhitening cannot respond to sharp changes in the power spectrum and hence can artificially "smooth" power estimates.

Conventional spectral estimators suffer from large variance in their estimates. That is, an increased data set length does not reduce the error on an individual power estimate. This is a fundamental property of Fourier transform estimators. It can be overcome using WOSA techniques, but again with a significant loss of spectral resolution and lowest measured frequency.

Multitaper spectral estimates alleviate both leakage and variance problems. The essence of the technique is the construction of a set of orthogonal data tapers, each of which has low leakage properties. Because each taper is orthogonal, spectral estimates of the data set windowed with each taper are statistically independent. These estimates can then be averaged to produce a final estimate with good leakage properties and considerably lowered variance.

Construction of an orthogonal set of data tapers can be challenging. In this work, the commonly used discrete prolate spheroidal surfaces (DPSS) functions are used, as calculated using Matlab™ 5.3 routines.

An important parameter for multitaper spectral estimation is the bandwidth product, NW, which is related to the width of the kernel in frequency space. For a given NW, 2NW orthogonal data tapers exist. Higher NW values reduce leakage and variance, but at the expense of a reduced bandwidth. Throughout this work we use NW=4. This is higher than most uses of multitaper spectra, because it is the continuum spectrum that is of interest, not any sharp peaks within it.

As a result of this process spectral estimates for each interval for the *R*, *T*, and *N* components and the field magnitude were calculated, as a function of spacecraft frequency. In addition, total field component power was calculated as the sum of power in all three components for each frequency, resulting in five power spectra estimates for each interval. These spacecraft frequency power spectra were converted into plasma frame wavenumbers using Taylor's method [*Matthaeus and Goldstein*, 1982]. Since the plasma flow speed is much higher than any relevant wave speeds, fluctuations vary on much longer timescales than the time taken for them to be convected past the spacecraft. It is therefore possible to convert from spacecraft scales into the plasma frame. A given spacecraft frequency f corresponds to a spatial wavenumber $k = 2\pi f / V_{SW}$, where V_{SW} is the mean solar wind expansion velocity during the interval, which is much greater than the spacecraft velocity relative to the Sun. Conversion into plasma wavenumber effectively removes the effect of variations in solar wind velocity.

The aim of this paper is to measure the scale-dependent variation of power levels and spectral indices with latitude and distance in high-speed solar wind streams. It is therefore necessary to estimate powers and spectral indices on a range of scales. This was done by "binning" the power spectral estimates by wavenumber. A series of ranges or bins in wavenumber space were defined, each covering a factor of 1.5 in scale. For each wavenumber range, for every interval and all five power spectra, estimates were made of the power and spectral index in that

range. Power estimates were calculated as the mean of all power estimates with wavenumbers within the range. Spectral indices were calculated as the least squares fitted gradients of log-log values of power against wavenumber for all values within the range. Error estimates of these quantities were also calculated. Spectral index estimates derived from differences in binned power levels in different wavenumber ranges result in very similar results to those presented here.

To ensure that these estimates were not dominated by points at extreme edges of a wavenumber range, no estimates were made for ranges which did not lie entirely between the maximum and minimum wavenumbers of a given estimated power spectrum. That is, wavenumber ranges at the high and low ends of the power spectra were discarded.

A typical calculated power spectrum and the resulting power spectral estimates in a number of wavenumber ranges are shown in Figure 2, along with spectral index estimates. While the binning procedure described above dramatically reduces the amount of data for each power spectral estimate, it still retains important information about the general amplitude and shape of the spectrum. The binned estimates of power levels and spectral indices are used throughout the rest of this work.

4. Power Variations in the Polar Heliosphere

Variations in magnetic field power levels with solar distance as measured by Ulysses during the northern polar pass are shown in Figure 3. Power in fluctuations in the wavenumber range 0.99-1.5 x 10^{-5} km^{-1} are shown for the the field components and the magnitude. Bulk solar wind speed and solar latitude are also shown; the latitude dependence of solar wind speed is clear, with slightly higher velocities at higher latitudes [*Phillips et al.*, 1995b].

The general decrease in power levels with solar distance is clear in Figure 3. In addition, the dramatically lower level of fluctuations in the field magnitude compared to all three components is visible, reflecting the fact that the fluctuations are highly Alfvénic on these scales in the polar heliosphere [e.g., *Goldstein et al.*, 1995]. The large-scale anisotropy of the fluctuations, with lower power in the radial component than in the other two components, reflecting the approximately radial minimum variance direction, is also clear [*Forsyth et al.*, 1996b].

The log-log dependence of power on distance shown in Figure 3 is close to linear, but it is not exactly so. That is, the power estimates shown in Figure 3a are not well described by a straight line. In fact, power decreases more rapidly at smaller solar distance on the log-log scale of Figure 3 than at larger distances: The line "dips." This nonlinear variation can be interpreted in two ways: as evidence of non-power-law dependence of power with distance or as a latitude effect. While it is impossible, given the orbit of Ulysses, to unambiguously distinguish latitude and distance variations, detailed consideration of the data suggests that the nonlinear variation in Figure 3 is due to a variation in latitude of the spacecraft: that is, that there is a slight latitude dependence of magnetic field power in the polar heliosphere. This analysis is described below.

A least squares fit of magnetic field power variations to both latitude and distance has been performed on a scale-by-scale basis for both northern and southern polar pass data. That is, for every wavenumber range, power estimates for all five data sets (R, T, and N components, field magnitude, and total component power) were fitted in a least squares sense to variations in latitude

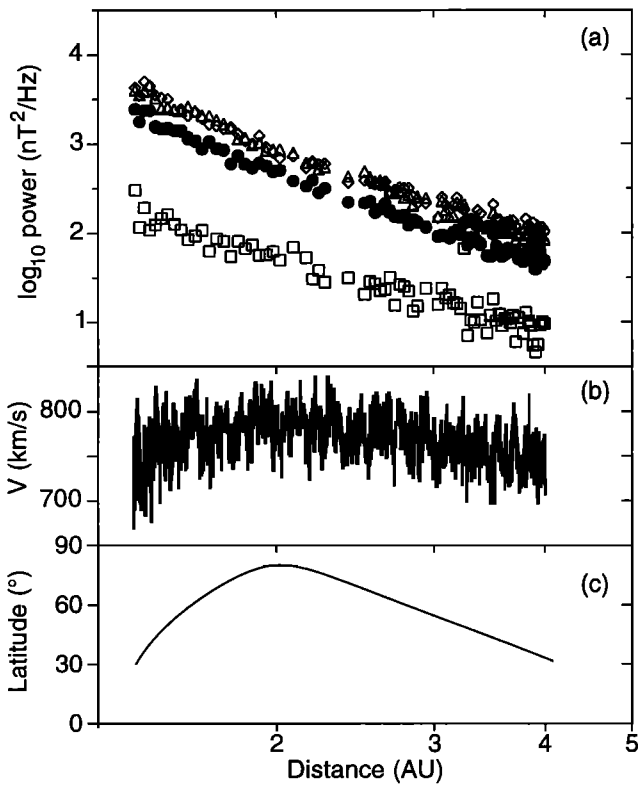

Figure 3. Variations in magnetic field power levels during the Ulysses northern polar pass, plotted as a function of solar distance. (a) power levels for all three components (R, solid circles; T, triangles; and N, diamonds) and field magnitude (squares); (b) radial solar wind speed; and (c) heliographic latitude. Power levels are shown for a wavenumber range of 0.99-1.5 x 10^{-5} km^{-1}.

and distance. In practice, a multiple linear regression method [see, e.g., *Bevington*, 1969, chap. 9] was used, fitting $\log_{10}$ power estimates to $\log_{10}$ Sun-spacecraft distance variations and linear variations in the sine of the absolute spacecraft heliolatitude (90° corresponds to the solar pole, 0° to the equator). Error estimates in power levels were not used, as errors associated with each power estimate were approximately constant in each wavenumber range, but the large number of power estimates (77 in the northern pass, 51 in the southern) allowed estimates of the errors associated with the linear fits to be made. At the end of this procedure, for each of the five data sets, for each polar pass, and for a set of wavenumber ranges, estimates of variations in power levels P of the form $\log_{10}P = A_p + B_p\log_{10} r + C_p\sin\theta$ were made, where r is the solar distance in AU and θ is the absolute heliolatitude.

In addition to multiple linear regression of power estimates the same procedure was performed on measured spectral index estimates α of the form $\alpha = A_\alpha + B_\alpha\log_{10} r + C_\alpha\sin\theta$ for each wavenumber range, resulting in values of A_α, B_α, and C_α for variations in spectral index with solar distance and latitude. Uncertainties in spectral index variations are naturally larger than those in the power because the spectral index is the derivative of power with wavenumber. The results of this analysis, the first scale-dependent estimate of the latitude and distance dependence of magnetic field fluctuations in the polar heliosphere near solar minimum, are presented in Figure 4. The panels correspond to

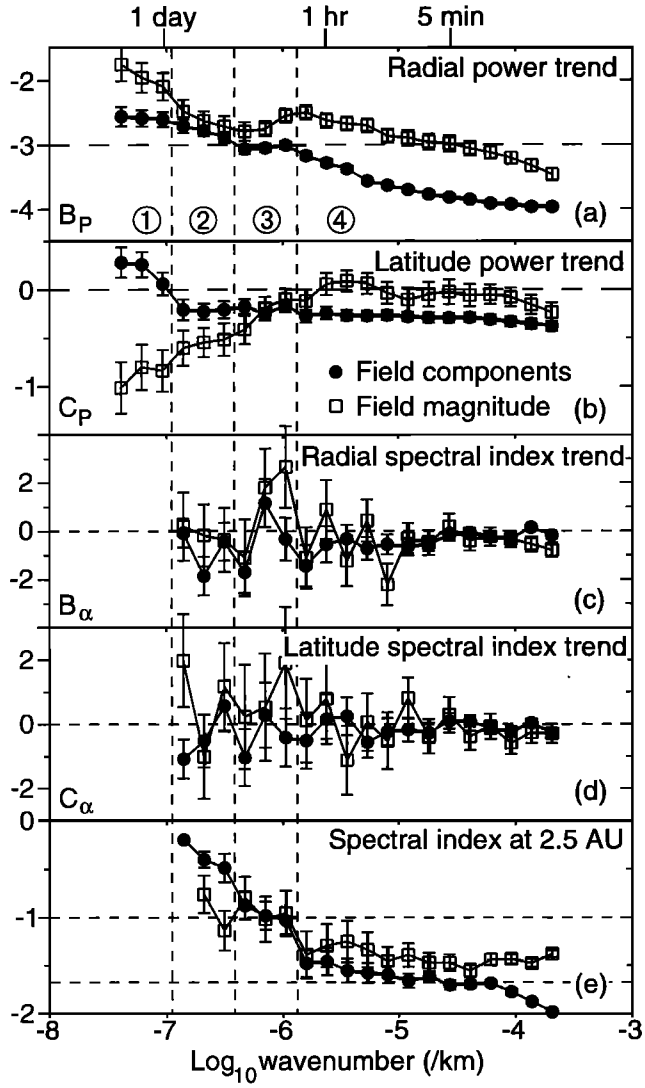

Figure 4. Scale-dependent variations of magnetic field power levels in the polar heliosphere. Wavenumber variations of (a) radial and (b) latitudinal power dependence, (c) radial (d) and latitudinal spectral index dependence, and (e) spectral index evaluated at 2.5 AU. Variations in power P and spectral index α were calculated from fits of the form $\log_{10}P = A_p + B_p \log_{10} r + C_p \sin\theta$ and $\alpha = A_\alpha + B_\alpha \log_{10} r + C_\alpha \sin\theta$. Data are shown for total component (solid circles) and field magnitude (open squares) power. Four wavenumber ranges are identified; these are discussed in the text. Approximate spacecraft timescales are marked, based on a 750 km s^{-1} solar wind speed.

parameters B_P and C_P (radial and latitudinal variations) for power variations (Figures 4a and 4b); B_α and C_α for spectral index variations (Figures 4c and 4d); and values of the spectral index α estimated from a distance fit for a distance of 2.5 AU (Figure 4e). The spectral index provides context information and illustrates the transition between small-scale turbulence and larger-scale waves.

On the basis of the spectral index and latitudinal and radial power scalings it is possible to identify a number of discrete ranges of scales, which are marked on Figure 4. Range 1, at the largest scales, is characterized by a radial power decrease slower than WKB (that is, larger than -3) and a positive latitudinal power dependence of the field components (that is, higher power at higher latitudes), and the opposite in the field magnitude. This range extends to the largest scales measured, where it is not possible to reliably measure the spectral index, to ~10^{-7} km^{-1}, around 23 hours in the spacecraft frame.

Range 2 extends from around 10^{-7} to around 4×10^{-7} km^{-1}. On these scales the decrease in power with distance for both the components and the magnitude of the field is more rapid with increasing wavenumber. In addition, the latitudinal component power trend is negative, as it is at all smaller scales, implying lower power at higher latitudes. The spectral index of the field components on these scales is near -0.5 but appears to tend toward 0 at larger scales.

Within range 3, covering wavenumbers from ~4×10^{-7} to 10^{-6} km^{-1}, power levels decrease with distance approximately as $P \propto r^{-3}$, the WKB value [e.g., *Bazer and Hurley*, 1963], and the spectral index is near -1 for both components and the magnitude. These scales can be easily interpreted as indicative of Alfvén waves, as seen at low latitudes [e.g., *Marsch and Tu*, 1990]. Indeed, Roberts [1989] showed that radial variations of fluctuations on these scales at low latitudes are consistent with WKB behavior. Latitude variations in the magnitude, slightly negative, are similar to those in the components.

Range 4 covers all wavenumbers from around 10^{-6} km^{-1} upward to the smallest scales measured in this work. On these scales, power levels in the components decrease with distance more rapidly than WKB, an effect that is more pronounced at higher wavenumbers, where the radial scaling appears to tend to a value near -4. This faster than WKB power decrease is consistent with a turbulent cascade, as seen at low latitudes and previously inferred from changes in the spectral index in Ulysses polar data by *Horbury et al.* [1996]. Indeed, Figure 4c shows that while estimates of radial trends in the spectral index are generally very noisy, the only scales on which there is a consistent deviation from zero are those around 10^{-6} km^{-1} and above, where there is a trend for values of the spectral index of the field components to decrease with distance. This is as expected for the low-frequency end of a turbulent cascade, where the spectrum is gradually steepening, and is consistent with trends in the spectral index described by *Horbury et al.* [1996]. The spectral index of the field components on these scales is significantly less than -1 and tends toward -5/3 with increasing wavenumber.

On the basis of the above results, range 4 can therefore be identified as a turbulent cascade, whose small-scale end is approximately an inertial range. However, range 4 also displays some other characteristics. While radial and latitudinal variations in the field magnitude and components are similar to measurement errors within range 3, they are different in range 4. There is no significant latitude trend in the magnitude, while it persists on all scales of range 4 in the components. Radial field magnitude power variations are much lower than those in the component: Typically, the difference is around 0.8, corresponding to a relative difference in diminution over a tenfold distance change of a factor of around 6. The spectral index of the field magnitude is consistently higher, that is, the spectrum is flatter, than the components throughout range 4. Above around 10^{-4} km^{-1} (around 100 s in the spacecraft frame) the spectrum of the field components steepens significantly. This may be a result of the 12 s boxcar averaging used in this work but may also reflect the high-frequency termination of the MHD regime or the presence of interstellar pickup proton cyclotron waves [*Murphy et al.*, 1995], since this scale is near the local proton gyrofrequency.

On the basis of Figure 4, therefore, it is possible to identify a number of ranges of scales with distinct behavior: a population of $1/f$ waves, which are known to be Alfvénic [e.g., *Goldstein et al.*, 1995] and decrease in power with distance as WKB: this is range 3. At higher wavenumbers (range 4) there is a turbulent cascade with a spectral index of the field components near -5/3 and a faster than WKB power decrease. At lower wavenumbers, (ranges 1 and 2) power decreases less rapidly than WKB, and the spectrum is flatter.

The large number of parameters in Figure 4, and their complex scale-dependent variations, makes it difficult to discuss one scale or parameter without considering the others. In the detailed discussion of the data in sections 4.1-4.5, latitude variations in power levels are considered first, before a discussion of each range of scales in turn.

4.1 Latitude Variations in Field Components: Coronal Overexpansion

A remarkable result of the analysis presented in this paper is the latitudinal variations in power levels shown in Figure 4b. On all scales smaller than around 10^{-7} km^{-1} (~1 day in the spacecraft frame) there is a consistent, negative dependence of field component power on latitude. There is a slight tendency for this to be larger at smaller scales, although this may be an artefact of the analysis method. The latitudinal power dependence value C_P is around -0.3. Recall that this is the dependence of $\log_{10}$ power on $\sin\theta$. A value of C_P around -0.3 corresponds to power at 80° being around 30% lower than that at 30°. This is a significant reduction which has consequences for energetic particle propagation, a topic which is discussed in section 5.

What, then, is the cause of this large power reduction at the highest latitudes? The fact that it is present in range 3, which is populated by Alfvén waves which are essentially unchanged since leaving the upper corona, implies that the latitudinal variation is "imprinted" on the fluctuations by the time they reach the source surface, where the solar wind flow becomes nearly radial.

Conditions within coronal holes, from which high-speed streams originate, are known to be remarkably homogeneous at the large scale, at least away from their boundaries. It seems unlikely, therefore, that the power variation observed is the result of a latitudinal variation in the generation of the fluctuations within coronal holes. Similarly, there is no obvious mechanism within the solar wind at a distance comparable to Ulysses' orbit to produce such a change in power levels. The lack of a significant latitudinal gradient in the spectral index on all measured scales indicates that the latitudinal power dependence is not likely to be due to more rapid turbulent development at higher latitudes: The spectral index is a sensitive indicator of whether energy transfer between scales is taking place, so the lack of a latitude trend suggests that the energy transfer rate is the same at all measured latitudes.

The expected latitudinal independence of fluctuation power in the low corona and the lack of a mechanism for producing a latitudinal variation in power at several AU suggest that the observed variations are generated between the lower corona and the source surface. A natural cause of such a variation is coronal hole overexpansion.

It is well known that high-speed solar wind from coronal holes "overexpands" to cover a much larger solid angle at several solar radii than the coronal holes cover in the lower corona. This superradial expansion is driven by the higher pressure in coronal holes and acts to equalize the magnetic field pressure, as demonstrated by *Smith and Balogh* [1995], who showed that the radial field component is, on average, independent of latitude in the heliosphere near solar minimum.

Near solar minimum the Sun's large-scale magnetic field is dominated by the dipolar term, leading to a higher magnetic field strength at higher latitudes. As a result, the expansion factor, the ratio of the solid angle subtended by a fluid packet at the source surface to that in the lower corona or photosphere, is greatest at higher latitudes, even within a coronal hole. Note that the expansion factor between the photosphere and 2.5 solar radii has the opposite dependence on latitude: For example, see Figure 5 of *Goldstein et al.* [1996].

Assuming a $\sin^7\theta$ dependence of photospheric magnetic field strength on latitude [e.g., *Wang and Sheeley*, 1995]; that only open flux from polar coronal holes expands to produce the solar wind; and that the coronal holes extend symmetrically from 90° to 70° heliolatitude in the photosphere leads to estimates of the expansion factor of 4.4 at 30° far from the Sun and 5.8 at 80° after magnetic pressure equalization. If the fluctuations obey WKB scaling during this expansion, likely in the upper corona for all the scales considered here, then the reduction in power as a result of the overexpansion is inversely proportional to the expansion factor. If fluctuation power in the lower corona is independent of latitude, the expansion factors above lead to a relative reduction in power between 80° and 30° at several AU of around 25%, equivalent to a $\sin\theta$ latitude gradient of -0.23, similar to that observed. Results of the analysis of the southern pass field data are similar. It seems likely, therefore, that the latitudinal gradient in component power levels at wavenumbers above 10^{-7} km^{-1} is due to coronal hole overexpansion. The ranges of scales identified in Figure 4 are now discussed in detail, beginning with the simplest, range 3.

4.2 Range 3: 4×10^{-7} - 10^{-6} km^{-1}

This range, as discussed in section 4, appears to be populated by Alfvénic fluctuations propagating antisunward [*Goldstein et al.*, 1995]. The spectral index is near -1, as also shown by *Horbury et al.* [1996], and power decreases with distance as r^{-3}, the WKB value. These fluctuations are similar to those seen at low latitudes in high-speed streams. There is no significant latitudinal or radial trend in spectral index, as expected. The spectral index of the waves is not changing with distance since they are essentially noninteracting. The nearly constant solar wind speed in high-latitude solar wind flows means that the time since waves were launched from the corona is a linear function of solar distance and has no latitudinal dependence. Given $1/f$ fluctuations over all dynamic scales close to the Sun in all high-speed flows, one would therefore expect the same wavenumber dependence of α at all latitudes at a given distance. This is in contrast to the latitude dependence of power levels, which are functions of both solar distance and source conditions: The latter are functions of latitude, resulting in a latitude dependence of power levels in the distant heliosphere. Behavior of the field magnitude on these scales is similar to that of the components in Figures 4a-e, probably because most magnitude fluctuations are the result of nonlinear variations in the large-amplitude Alfvén waves, rather than due to compressive wave modes.

The anisotropy of the fluctuations is of interest both for an understanding of MHD dynamics and of cosmic ray propagation. Figure 5 presents an analysis of anisotropy variations in the polar heliosphere using a similar method to that presented in Figure 4. For each interval and wavenumber range the ratio of power in

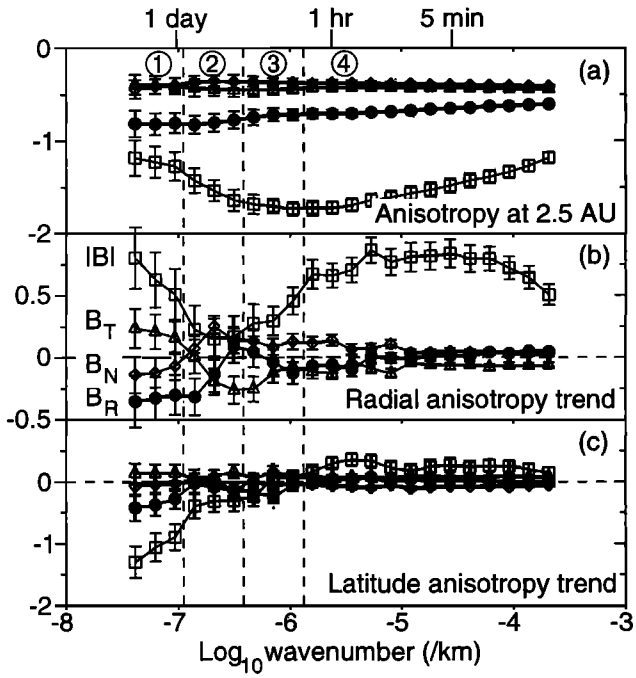

Figure 5. Scale dependence of power anisotropy in the polar heliosphere. Wavenumber variations of (a) $\log_{10}$ ratios of power in B_R (circles), B_T (triangles), B_N (diamonds), and $|B|$ (squares) to the trace of the power spectrum, at 2.5 AU; (b) radial variations in these values; and (c) latitudinal variations in these values.

each field component and the field magnitude to the total component power was calculated. Fits of base 10 logarithms of these values to variations in $\log_{10}r$ and $\sin\theta$ were performed in the same manner as those for the spectral index, producing estimates of the radial and latitudinal dependencies as functions of wavenumber. In addition, anisotropies were evaluated at 2.5 AU. Some of the variations in Figure 5, particularly in the field magnitude, can be deduced from Figure 4, but they are included in Figure 5 for reference.

Figure 5 shows that power in the field magnitude is nearly 2 orders of magnitude lower within range 3 than in the field components, a larger anisotropy than at any other scale, reflecting the dominance of the noncompressive Alfvén mode at these scales. There is no significant latitudinal anisotropy in any of the field components or the magnitude, while there is a small tendency for relative power in the magnitude to increase with distance, a trend that is more pronounced at higher wavenumbers in range 4 and is discussed in section 4.3.

Power in the radial component is significantly lower than in the two perpendicular components within range 3, a result previously discussed by *Forsyth et al.* [1996b], which implies that Alfvén waves in the polar heliosphere have radial minimum variance directions. It is remarkable that this power anisotropy is maintained across all measured scales in this analysis, however. At small scales, fluctuations are predominantly field-perpendicular [e.g., *Horbury et al.*, 1995]: The radial minimum power at these scales (e.g., $k > 10^{-5}$ km^{-1}) in this analysis is a result of the field more often being nearly radial during the long data intervals than close to the two flow-perpendicular directions. Power anisotropies at small scales are therefore affected by those at larger scales. These results are in contrast to earlier low-latitude observations [e.g., *Klein et al.*, 1991] which demonstrated a minimum variance direction of magnetic field fluctuations, even on relatively large scales (hours in the spacecraft frame) near the Parker spiral direction, which by several AU is essentially parallel to the T (tangential) direction. Fluctuations in range 3, then, are broadly as expected from low-latitude observations of Alfvén waves.

4.3 Range 4: 10^{-6} km^{-1} and Higher

At wavenumbers above around 10^{-6} km^{-1}, field component power decreases with distance more rapidly than r^{-3}, indicating the presence of a turbulent cascade and energy transfer to smaller scales. The spectrum steepens as expected, and there is therefore a negative trend in the spectral index with distance, at least in the field components: There is a large scatter in magnitude values, making the determination of a trend difficult.

The latitudinal dependence of the components seen in range 3 persists on these scales, consistent with power being transferred from larger scales: The cascade "inherits" the latitudinal power dependence of the fluctuations that are the source of the turbulence. The progressively more rapid radial power decrease with increasing wavenumber is consistent with a developing cascade, including scales which are not part of an inertial range. On the basis of changes in the spectral index with distance in the polar heliosphere, *Horbury et al.* [1996] predicted a $r^{-3.7}$ decrease of power with distance in the inertial range. Figure 4 shows that power scaling reaches a value near -4 as the spectral index reaches -5/3, a rather more rapid decrease than Horbury et al. predicted. A more rapid decrease in power at smaller scales implies a steepening of the power spectrum, and indeed, it appears that as the radial component power dependence with wavenumber tends to flatten toward -4, the spectral index tends to -5/3, and the radial spectral index trend tends toward 0. This only seems to occur around $k \sim 10^{-5}$ km^{-1} (although it is difficult to obtain precise measurements from the results presented here), implying that the range over which energy transfer occurs but an inertial range has yet to form covers at least an order of magnitude.

There are several remarkable aspects of the field magnitude fluctuations within the turbulent cascade revealed in Figure 4. First, power in the magnitude decreases much less rapidly with distance than the components on these scales: Indeed, magnitude power near 10^{-6} km^{-1} decreases more slowly than that at larger scales, at around 4×10^{-7} km^{-1}. There is a consistent difference of around 0.8 between the magnitude and component scalings as they both vary over range 4.

Second, there is no significant latitude variation in magnitude power levels, although such a variation persists in the components. Indeed, such a variation, even larger in magnitude, exists for magnitude fluctuations at even larger scales but is clearly not present within range 4. Finally, the magnitude spectral index is significantly higher (that is, the spectrum is shallower) than that of the components throughout range 4.

The causes of these unusual results are not clear. Two possibilities are discussed here, although neither satisfactorily agrees with all the data in Figure 4.

The first possible explanation for the field magnitude variations within range 4 is that they are due to compressive MHD fluctuations generated by the decay of Alfvén waves, through parametric decay for example. In this case, magnitude power would be generated at all scales smaller than the small-scale end of the $1/f$ regime, range 3. This is indeed what is shown in Figure 4a. The gradual increase in relative power in the magnitude with

increasing wavenumber (Figure 5a) is also consistent with this interpretation. However, the lack of a latitude gradient in magnitude power within range 4 is not consistent with this mechanism. Just as the latitude gradient in component power in the turbulent cascade is inherited from range 3, so compressive fluctuations generated by the cascade should vary with latitude in the same way. The lack of a magnitude power gradient within range 4 appears to rule out the interpretation of the slower magnitude power decrease being due to compressive modes generated by Alfvén wave decay.

A second possible explanation for the magnitude power behavior is that it is caused by small-scale compression and rarefaction due to small velocity variations, for example between adjacent flux tubes or small-scale microstreams [e.g., *Neugebauer et al.*, 1995]. However, since stream-stream collisions, and hence compressions and rarefactions, are weaker at higher latitudes, these variations should also generate a lower magnitude power at higher latitudes.

It is unlikely that interstellar pickup ions are responsible for these variations: Pickup ion cyclotron waves are more likely to enhance field component power rather than that in the magnitude; they are unlikely to extend to such low wavenumbers; and they are unlikely to result in such a broadband power enhancement. The cause of the radial and latitudinal power variations within the turbulent cascade therefore remains unclear.

4.4 Range 1: 10^{-7} km^{-1} and Lower

At the largest measured scales, power in both the field components and magnitude decreases more slowly than r^{-3} with distance. This is consistent with the presence of "structures" rather than waves or turbulence on these scales, as suggested by *Jokipii and Kóta* [1989]. While *Jokipii et al.* [1995] found r^{-2} scaling at very low frequencies (20 days) in the polar heliosphere, the power scaling at the lowest frequencies measured here is around $r^{-2.6}$. However, it appears that the power decrease is less steep with increasing scale, so at even larger scales, closer to those measured by Jokipii et al., scaling may indeed be r^{-2}. Indeed, the scale at which the transition from "waves" to "structures" should occur, $T_c=4\pi V_A/(V_{SW}{}^2)$ (V_A is the Alfvén speed), is around 1.4 days at 1 AU [*Jokipii et al.*, 1995] but is around 3 days at 2.5 AU in the polar heliosphere, rather larger than the largest scale in Figure 4. Range 1 may therefore represent a transition to a r^{-2} scaling regime, but this is not clear from the results presented here. Indeed, the dramatically slower power decrease of the field magnitude within range 1 than in range 3, slower than r^{-2}, suggests that compression and rarefaction are important on these scales. This is not surprising, since the largest scales measured here, corresponding to spacecraft timescales of around 2 days, are similar to the length scales of microstreams [*Neugebauer et al.*, 1995]. Microstreams typically exhibit velocity variations of several tens of km s^{-1} over several days. These variations should indeed lead to compressions and rarefactions as they collide, and are probably responsible for the markedly slower radial magnitude power decrease visible in Figure 4. The presence of a negative latitudinal magnitude power trend within range 1 supports this interpretation: Stream-stream variations should be lower at higher latitudes, leading to less compression and lower field magnitude variations. The field magnitude variations within range 1 may also be the signatures of pressure-balanced structures, which *Marsch and Tu* [1993] showed became progressively more important with increasing solar distance in high-speed streams.

The radial power trends within range 1 are similar to those found on similar scales, around 1 day in the spacecraft frame, at low latitudes by *Roberts et al.* [1990]. Roberts et al. found a slower than WKB decrease in power levels and a spectral index near -1. However, the spectral index changed to near -1.7 by 8 AU, implying energy transfer, and Roberts et al. interpreted the slower than WKB power decrease as being due to power generated by compressions and rarefactions resulting from stream-stream interactions. There is no evidence of a change in spectral index on the largest scales considered here, within rather large errors: This may simply be due to the smaller distance range (only up to 4.1 AU) covered in this work.

The presence of a positive latitudinal trend in field component power, in contrast to that within ranges 3 and 4, suggests that the slower than WKB power decrease within range 1 is not simply due to enhanced power within compression regions associated with microstream interactions. Indeed, Figure 5 shows that within range 1, power in the radial field component is lower relative to the flow-perpendicular components at higher latitudes. This is the expected signature of the field line random walk model of *Jokipii and Kóta* [1989], which enhances the flow-perpendicular components. Figure 5 also shows that the slower than WKB radial component power decrease is largely the result of a relative enhancement in the tangential component power, consistent with a winding of the field with distance due to the Parker spiral.

4.5 Range 2: 10^{-7} - 4×10^{-7} km^{-1}

Range 2 is perhaps the most confusing regime identified in Figure 4, since it shares properties with both ranges 1 and 3. Radial power trends within range 2 seem to exhibit a smoother transition with scale between ranges 1 and 3, and the component spectral index increases dramatically at wavenumbers below the large-scale end of range 3, suggesting that the spectrum flattens completely around 10^{-7} km^{-1} (it is not possible to obtain reliable spectral index estimates within range 1). Similarly, the latitude power trend in the field magnitude decreases monotonically with increasing scale through range 2. On the basis of these parameters, ranges 1 and 2 appear to be very similar, both being transitions to different behavior at larger scales. However, the transition from a negative latitudinal power trend to a positive one is remarkably sharp and occurs at the transition scale between ranges 1 and 2: It is on the basis of this chance that the two ranges are treated as separate in this paper. It is not clear why the latitudinal power trend transition is so sharp, nor why it occurs at a scale so much larger than that at which WKB scaling breaks down.

5. Consequences for Energetic Particles

The latitudinal variation in power levels in the polar heliosphere near solar minimum has implications for energetic particle diffusion. The field-perpendicular diffusion coefficients are essentially proportional to the field-perpendicular power levels [e.g., *Jokipii*, 1966]. However, most cosmic ray modeling (see, e.g., *Potgieter* [1998] for a recent review) assumes that power levels, and hence diffusion coefficients, are simply proportional to $1/|B|$. The results presented here show that this assumption of the dependence of power levels on the field magnitude is not valid in the polar heliosphere and that significant latitude gradients, corresponding to differences of around 30% between 30° and 80°, exist near solar minimum. The presence of latitudinal gradients in diffusion coefficients is necessary to drive the

drift of energetic particles between latitudes. Significant latitudinal gradients in energetic particle fluxes, both of galactic cosmic rays and the anomalous component, have been observed [e.g., *McKibben et al.*, 1996]. During the $A>0$ solar cycle minimum (that is, when northern solar magnetic fields were predominantly outward), when Ulysses traversed the polar heliosphere, ions traveled into the heliosphere through the polar regions and were therefore susceptible to latitudinal gradients in diffusion coefficients.

It is interesting to note that the rigidity-dependent latitude gradients observed [*McKibben et al.*, 1996] could be caused by scale-dependent variations in latitude gradients of power levels, as demonstrated in this paper, since high-rigidity particles resonate with larger-scale fluctuations than those at lower energies. Unfortunately, the energetic particle population at several AU is affected by scattering in the distant heliosphere. While it is possible to propagate the observed power spectra outward a short distance past Ulysses' orbit, it is not clear how certain aspects of the spectrum, such as the scale at which WKB scaling breaks down and "structures" dominate, will alter with distance and latitude. It is therefore difficult to construct a full scale, distance, and latitude-dependent description of power levels at this time. However, such a description is essential for an understanding of energetic particle propagation in the heliosphere, and a future paper will address this issue.

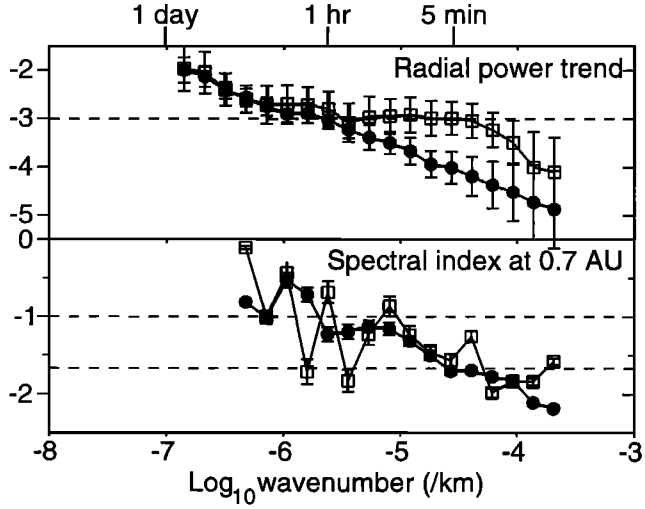

Figure 6. Scale-dependent variations of magnetic field power levels in high-speed streams at low latitudes, between 0.3 and 1 AU. Wavenumber variations of (top) radial power dependence and (bottom) spectral index evaluated at 0.7 AU. Data are shown for total component (solid circles) and field magnitude (open squares) power. Approximate spacecraft timescales are marked, based on a 750 km s^{-1} solar wind speed.

6. High-Speed Streams at Low Latitudes

The development of fluctuations within high-speed streams as they travel away from the Sun at low heliolatitudes has been well studied using data from the Helios 1 and 2 spacecraft, which repeatedly traveled between 0.3 and 1 AU. However, it is of interest to compare power scaling and spectral index variations directly between low-latitude (Helios) and high-latitude (Ulysses) observations using the same analysis techniques. To this end, we have analyzed 8 s averaged magnetic field data from the Helios 1 search coil magnetometer experiment [*Neubauer et al.*, 1977]. These data were purchased from the National Space Science Data Center and cover the period day 344, 1974 to day 121, 1976, with several large data gaps and numerous smaller ones. As with the Ulysses data, data gaps were linearly interpolated, although intervals were retained that contained up to 10% data gaps to produce a sufficient number of intervals from which to calculate trends. Similar least squares fits were made to power levels and spectral indices as discussed in section 3, but because of the limited latitude range covered by the Helios spacecraft, with a maximum heliolatitude of around 7°, the fits were made just to solar distance and not to latitude: The method employed here is not sufficiently sensitive to distinguish trends over such a small latitude range. In addition, 2 day intervals were used (rather than 5 days for Ulysses) to better ensure that each interval was within a single solar wind stream.

It is desirable to select intervals of Helios data taken entirely within high-speed, coronal hole flows at low latitudes to provide a consistent comparison with Ulysses polar measurements. Such intervals were identified using hourly averaged radial bulk plasma velocity measurements. A 2 day interval of data was considered to be within a high-speed stream if the velocity remained between 550 and 900 km s^{-1} for the entire interval duration. This procedure resulted in 29 valid intervals of data, covering the entire distance range from 0.3 to 1.0 AU. This selection criterion has significant drawbacks (it does not eliminate fast transients such as coronal mass ejections and could include some interaction regions), but it has the advantage of being simple to calculate. In practice, the inclusion of intervals which contain transients or interaction regions produces scatter in power estimates. This variation increases with solar distance as interaction regions develop but does not appear to alter estimates of power scalings within the accuracies of the method. However, these variations result in a rather larger scatter in values than with Ulysses polar data and hence larger errors in some fitted quantities. In particular, spectral index scaling estimates are too noisy to be of use. Figures 6 and 7 present the more reliable parameters for Helios data in a similar format to Figures 4 and 5 for Ulysses: radial power scaling, spectral index at 0.7 AU, anisotropy at 0.7 AU, and radial anisotropy scalings.

It is clear that the Ulysses and Helios results are similar. In particular, it is possible to identify an equivalent to Ulysses range 3, with WKB power scaling, a spectral index near -1, and very low relative magnitude power, at scales above around 10^{-6} km^{-1}, although the component spectral index is near -1.2 (and rather variable) and the magnitude spectral index is too variable to be useful.

At smaller scales, lower spectral indices, faster radial component power decreases and low field magnitude anisotropy are also visible, as for the turbulent cascade at high latitudes. There is a similar slower decrease in magnitude power, although the radial scaling never increases above -3, in contrast to that at higher latitudes.

At the largest scales a slower than WKB power decrease and more equal component and magnitude power are also similar to polar observations of structures. The considerably lower power in the radial field component within polar data is also present at low latitudes over all measured scales.

A clear difference between low- and high-latitude observations is the significant positive radial anisotropy trend visible in Figure 7 for the radial field component, corresponding to a higher relative power level with distance. This trend covers all scales above ~10^{-6} km^{-1}, in other words, all scales that appear wave-like

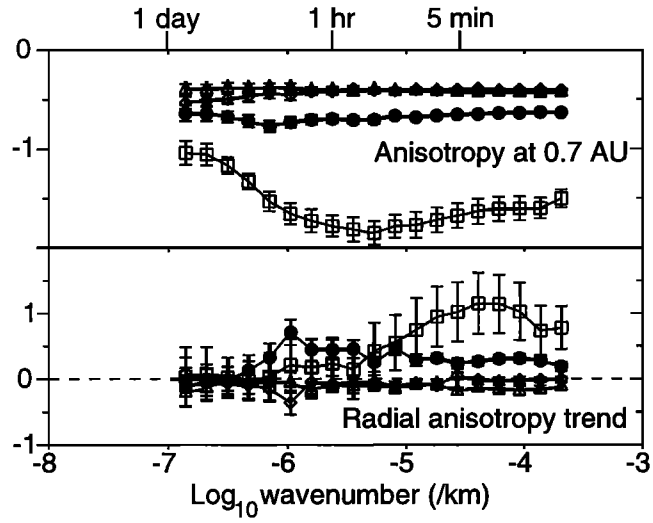

Figure 7. Scale dependence of power anisotropy in high-speed streams at low latitudes. Wavenumber variations of (top) $\log_{10}$ ratios of power in B_R (circles), B_T (triangles), B_N (diamonds) and $|B|$ (squares) to the trace of the power spectrum, at 2.5 AU; and (bottom) radial variations in these values. Approximate spacecraft timescales are marked, based on a 750 km s^{-1} solar wind speed.

or turbulent rather than due to structures, but it is not present in the polar data. This is surprising since absolute anisotropy levels for the radial field component are similar at 0.7 and 2.5 AU. This trend may simply reflect an increasing field-aligned anisotropy level with distance, in agreement with some earlier low-latitude studies [e.g., *Bavassano et al.*, 1982a] but not others at both low [*Klein et al.*, 1993] and high latitudes [*Horbury et al.*, 1995]. However, one referee has suggested that this variation may be due to the change in average field direction from near radial at 0.3 AU to nearer 45° by 1 AU, which, since the minimum variance direction is generally aligned with the mean field, would result in a corresponding increase in relative radial power levels with distance, as observed.

As is well known [e.g., *Bavassano et al.*, 1982b], the decay of low-frequency Alfvén waves and development of the turbulent cascade gradually moves the transition or breakpoint scale, essentially the small-scale termination of the $1/f$ regime, to larger scales with increasing distance. *Horbury et al.* [1996] measured the rate of movement of the breakpoint scale with distance in the polar high-speed wind as $k \propto r^{1.1\pm0.1}$ and showed that the breakpoint scale at 0.3 AU in low-latitude high-speed wind was consistent with that seen in the polar heliosphere at several AU on the basis of this evolution rate. It is not possible to make such precise measurements of the breakpoint scale movement with the methods used in this work, but an approximate consistency check can be made. A crude measure of the breakpoint scale is the wavenumber at which the field magnitude anisotropy is most significant: This appears from Figures 5 and 7 to correspond to the high-frequency termination of the $1/f$ regime. At 2.5 AU this scale is around $k\sim10^{-5.9}$ km^{-1}, and at 0.7 AU, $k\sim10^{-5.3}$ km^{-1}. This corresponds to a radial trend in the breakpoint scale of $k\propto r^{1.1}$, consistent with the *Horbury et al.* [1996] measurement.

6.1 Comparison of Low- and High-Latitude Power Levels

In addition to comparing power scalings at low and high latitudes, it is of interest to compare absolute power levels. Unfortunately, the Ulysses and Helios orbits do not overlap in distance, so a direct comparison at a particular distance cannot be made. However, given measurements of the radial power scalings, estimates of the power spectrum at distances outside the range covered by the spacecraft can be made, by "propagating" observed spectra to that distance. Given the greater uncertainty in the Helios measurements than in those from Ulysses, the distance chosen for this comparison is 1 AU, being closer to the Helios orbit than the Ulysses one. Figure 8 shows component and magnitude power spectra at 1 AU as estimated from Ulysses (solid lines) and Helios (dashed lines) data. The general agreement is remarkably good, in both shape and amplitude, particularly at around $k\sim10^{-6}$ km^{-1}, where waves predominate at both Helios and Ulysses, and so power scalings are similar. At larger scales there is a pronounced enhancement in magnitude power in the Helios data relative to Ulysses, probably due to the presence of compressive structures at low latitudes. Between 10^{-6} and 10^{-5} km^{-1}, magnitude power estimates from both spacecraft are astonishingly close. This result, combined with the lack of a latitude trend in magnitude power on these scales, suggests that there may be a background spectrum of magnitude power in high-speed wind at these scales, at all latitudes. However, its cause remains unclear.

Helios power estimates are generally lower than those from Ulysses in Figure 8. However, as discussed in section 4.1, variable coronal hole expansion factors can alter power levels. Therefore one would expect variations in power levels, perhaps up to a factor of 2, between streams from different coronal holes and, indeed, even within flows from a single hole. Perhaps more interesting is the rather steeper spectrum derived from the Helios data. On the basis of previous estimates of the breakpoint scale at low latitudes, from 0.3 to 10 AU, *Horbury et al.* [1996] suggested that high-latitude fluctuations developed more slowly than those

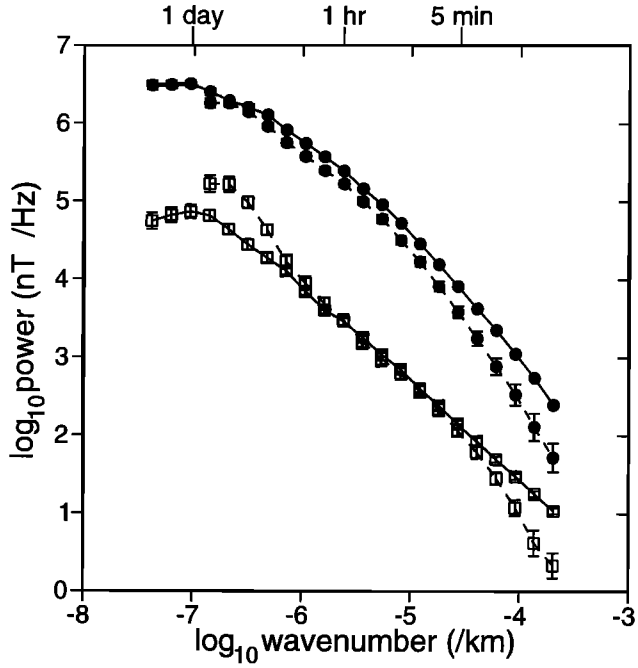

Figure 8. Power spectrum of field components (solid circles) and magnitude (squares) in high-speed wind at 1 AU estimated from trends in power scalings at Ulysses between 1.4 and 4.1 AU (solid lines) and Helios between 0.3 and 1.0 AU (dashed lines). Approximate spacecraft timescales are marked, based on a 750 km s^{-1} solar wind speed.

at low latitude, probably because of the lack of large-scale stream structure at high latitudes, an idea previously proposed by *Roberts* [1990], *Grappin et al.* [1991], and *Bruno* [1992] and recently supported by *Bavassano et al.* [1998] using midlatitude Ulysses data. The steeper power spectrum derived from low-latitude data is consistent with this result, again suggesting that MHD turbulence can be "driven" by a disturbed environment.

7. Conclusions

This paper presents the first scale-dependent estimates of the dependence of magnetic field power levels and spectral indices on latitude and distance in high-speed solar wind in the high-latitude heliosphere between 1.4 and 4.1 AU near solar minimum, as well as a similar analysis of low-latitude high-speed wind fluctuations between 0.3 and 1 AU. None of the results are contradictory to the accepted view of magnetic field fluctuations on MHD scales in the heliosphere, but several are new and have important consequences: (1) A significant reduction in field component power with increasing latitude over a wide range of scales, probably as a result of coronal hole overexpansion. (2) In contrast, lack of a latitude gradient in field magnitude power accompanied by a dramatic relative enhancement in magnitude power with distance, but only within the turbulent cascade, for which the authors have no explanation consistent with all measured parameters. (3) A measurement of the scale at which the transition from waves and turbulence to "structures" occurs (k~10^{-7} km^{-1}). At larger scales there is a much smaller power decrease and significantly lower magnitude power (and higher component power) at higher latitudes. (4) The presence of all the radial trends observed in the Ulysses data in the low- latitude data, despite the presence of strong velocity shears, compressions, and rarefactions near the ecliptic, which affect the turbulence at larger distances from the Sun. (5) Close agreement between power levels in high-speed streams at low and high latitudes. These results place strong constraints on theories and models of the development of MHD turbulence. It is hoped that current models will be revisited in light of these observations, in particular, the field magnitude variations, and shed some light on the processes that produce them.

Power variations with distance and latitude affect energetic particle diffusion coefficients. In particular, latitude trends in power levels can induce latitudinal transport in energetic particles in the polar heliosphere. A full description of power levels in the distant heliosphere, and hence diffusion coefficients, will be developed in a later work. Such a description is vital for attempting to match observed particle fluxes with current models.

Acknowledgments. T. S. Horbury is grateful to F. Neubauer for useful discussions regarding Helios data and N. L. Sheeley for clarification of coronal hole expansion factors. A CD-ROM of Helios magnetic field data was purchased from the National Space Science Data Center. This work was supported in part by PPARC (UK) grant GR/L29903.

Janet G. Luhmann thanks D. Aaron Roberts and Roland Grappin for their assistance in evaluating this paper.

References

Balogh, A., T. J. Beek, R. J. Forsyth, P. C. Hedgecock, R. J. Marquedant, E. J. Smith, D. J. Southwood, and B. T. Tsurutani, The magnetic field investigation on the Ulysses mission: Instrumentation and preliminary scientific results, *Astron. Astrophys. Suppl. Ser., 92,* 221–236, 1992.

Balogh, A., E. J. Smith, B. T. Tsurutani, D. J. Southwood, R. J. Forsyth, and T. S. Horbury, The heliospheric magnetic field over the south polar region, *Science, 268,* 1007-1010, 1995.

Bavassano, B., M. Dobrowolny, G. Fanfoni, F. Mariani, and N. F. Ness, Statistical properties of MHD fluctuations associated with high-speed streams from Helios-2 observations, *Sol. Phys.,* 78, 373-384, 1982a.

Bavassano, B., M. Dobrowolny, F. Mariani, and N. F. Ness, Radial evolution of power spectra of interplanetary Alfvénic turbulence, *J. Geophys. Res., 87,* 3617–3622, 1982b.

Bavassano, B., E. Pietropaolo, and R. Bruno, Cross-helicity and residual energy in solar wind turbulence: Radial evolution and latitudinal dependence in the region from 1 to 5 AU, *J. Geophys. Res., 103,* 6521-6529, 1998.

Bazer, J., and J. Hurley, Geometrical hydromagnetics, *J. Geophys. Res., 68,* 147-174, 1963

Bevington, P. R., *Data Reduction and Error Analysis for the Physical Sciences,* McGraw-Hill, New York, 1969.

Bruno, R., Inner heliosphere observations of MHD turbulence in the solar wind: Challenges to theory, in *Solar Wind Seven,* ed. E. Marsch and R. Schwenn, pp 423-428, Pergamon, Tarrytown, N Y., 1992.

Forsyth, R. J., A. Balogh, T. S. Horbury, G. Erdos, E. J. Smith, and M. E. Burton, The heliospheric magnetic field at solar minimum: Ulysses observations from pole to pole, *Astron. Astrophys., 316,* 287-295, 1996a.

Forsyth, R. J., T. S. Horbury, A. Balogh, and E. J. Smith, Hourly variances of fluctuations in the heliospheric magnetic field out of the ecliptic plane, *Geophys Res. Lett., 23,* 595-598, 1996b.

Goldstein, B. E., E. J. Smith, A. Balogh, T. S. Horbury, M. L. Goldstein, and D. A. Roberts, Properties of magnetohydrodynamic turbulence in the solar wind as observed by Ulysses at high heliographic latitudes, *Geophys. Res. Lett., 22,* 3393-3396, 1995.

Goldstein, B. E., M. Neugebauer, J. L. Phillips, S. Bame, J. T. Gosling, D. McComas, Y.-M. Wang, N. R. Sheeley, and S. T. Suess, Ulysses plasma parameters: Latitudinal, radial, and temporal variations, *Astron. Astrophys., 316,* 296-303, 1996.

Goldstein, M. L., and D. A. Roberts, Magnetohydrodynamic turbulence in the solar wind, *Annu. Rev. Astron. Astrophys., 33,* 283-325, 1995.

Grappin, R., M. Velli, and A. Mangeney, Alfvénic versus standard turbulence in the solar wind, *Ann. Geophys., 9,* 416-426, 1991.

Horbury, T. S., A. Balogh, R. J. Forsyth, and E. J. Smith, Anisotropy of inertial range turbulence in the polar heliosphere, *Geophys. Res. Lett., 22,* 3405-3408, 1995.

Horbury, T. S., A. Balogh, R. J. Forsyth, and E. J. Smith, The rate of turbulent evolution over the Sun's poles, *Astron. Astrophys., 316,* 333-341, 1996

Jokipii, J. R., Cosmic-ray propagation, I, Charged particles in a random magnetic field, *Astrophys. J., 146,* 480-487, 1966.

Jokipii, J. R., and J. Kóta, The polar heliospheric magnetic field, *Geophys. Res. Lett., 16,* 1-4, 1989.

Jokipii, J. R., J. Kóta, J. Giacalone, T. S. Horbury, and E. J. Smith, Interpretation and consequences of large-scale magnetic variances observed at high heliographic latitude, *Geophys. Res. Lett., 22,* 3385-3388, 1995.

Klein, L. W., D. A. Roberts, and M. L. Goldstein, Anisotropy and minimum variance directions of solar wind fluctuations in the outer heliosphere, *J. Geophys. Res., 96,* 3779-3788, 1991.

Klein, L., R. Bruno, B. Bavassano, and H. Rosenbauer, Anisotropy and minimum variance of magnetohydrodynamic fluctuations in the inner heliosphere, *J. Geophys. Res., 98,* 17,461-17,466, 1993.

Marsch, E., and C.-Y. Tu, On the radial evolution of MHD turbulence in the inner heliosphere, *J. Geophys. Res., 95,* 8211-8229, 1990.

Marsch, E., and C.-Y. Tu, Correlations between the fluctuations of pressure, density, temperature and magnetic field in the solar wind, *Ann. Geophys., 11,* 659-677, 1993.

Matthaeus, W. H., and M. L. Goldstein, Measurement of the rugged invariants of magnetohydrodynamic turbulence in the solar wind, *J. Geophys. Res., 87,* 6011-6028, 1982.

Matthaeus, W. H., and M. L. Goldstein, Low-frequency 1/*f* noise in the interplanetary magnetic field, *Phys. Rev. Lett.,* 57, 495–502, 1986.

Matthaeus, W. H., J. W. Bieber, and G. P. Zank, Unquiet on any front: Anisotropic turbulence in the solar wind, *Rev. Geophys., 33,* 609-614, 1995.

McKibben, R. B., J. J. Connell, C. Lopate, J. A. Simpson, and M. Zhang, Observations of galactic cosmic rays and the anomalous helium during Ulysses passage form the south to north solar pole, *Astron. Astrophys., 316,* 547-554, 1996.

Murphy, N., E. J. Smith, B. T. Tsurutani, A. Balogh, and D. J. Southwood, Further studies of waves accompanying the solar wind pick-up of interstellar hydrogen, *Space Sci. Rev., 72,* 447-453, 1995.

Neubauer, F. M., H. J. Beinroth, H. Barnstorf, and G. Dehmel, Initial results from the Helios-1 search-coil magnetometer experiment, *J. Geophys*, *42*, 599-614, 1977.

Neugebauer, M, B.E. Goldstein, D J. McComas, S.T. Suess, and A. Balogh, Ulysses observations of microstreams in the solar wind from coronal holes, *J Geophys Res*, *100*, 23,389-23,395, 1995.

Percival, D B., and A. T. Walden, *Spectral Analysis for Physical Applications*, Cambridge Univ Press, New York, 1993.

Phillips, J L, S. J Bame, W. C. Feldman, B. E. Goldstein, J. T. Gosling, C. M. Hammond, D. J. McComas, M. Neugebauer, E. E. Scime, and S. T. Suess, Ulysses solar wind plasma observations at high southerly latitudes, *Science*, *268*, 1030-1033, 1995a.

Phillips, J. L., et al., Ulysses solar wind observations from pole to pole, *Geophys. Res. Lett.*, *22*, 3301-3304, 1995b.

Potgieter, M S., The modulation of galactic cosmic rays in the heliosphere: Theory and models, *Space Sci. Rev*, *83*, 147-158, 1998.

Roberts, D A, Interplanetary observational constraints on Alfvén wave acceleration of the solar wind, *J. Geophys. Res.*, *94*, 6899-6905, 1989.

Roberts, D. A., Turbulent heliospheric fields, *Geophys Res. Lett.*, *17*, 567-570, 1990.

Roberts, D A., M. L. Goldstein, L. W. Klein, and W. H. Matthaeus, Origin and evolution of fluctuations in the solar wind: Helios observations and Helios-Voyager comparisons, *J. Geophys. Res.*, *92*, 12,023-12,035, 1987.

Roberts, D. A., M. L. Goldstein, and L. W. Klein, The amplitudes of interplanetary fluctuations: Stream structure, heliocentric distance, and frequency dependence, *J. Geophys. Res.*, *95*, 4203-4216, 1990.

Smith, E. J., and A. Balogh, Ulysses observations of the radial magnetic field, *Geophys Res Lett.*, *22*, 3317-3320, 1995.

Tu, C -Y., and E. Marsch, MHD structures, waves and turbulence in the solar wind· Observations and theories, *Space Sci Rev.*, *73*, 1-210, 1995

Tu, C.-Y., Z.-Y Pu, and F.-S. Wei, The power spectrum of interplanetary Alfvénic fluctuations: Derivation of the governing equation and its solution, *J. Geophys. Res.*, *89*, 9695-9702, 1984.

Wang, Y.-M, and N. R. Sheeley Jr., Solar implications of Ulysses interplanetary field measurements, *Astrophys. J.*, *447*, L143-L146, 1995.

T. S. Horbury, and A. Balogh, The Blackett Laboratory, Imperial College, London SW7 2BW, United Kingdom (a.balogh@ic.ac.uk; t.horbury@ic ac uk)

(Received May 2, 2000, revised July 21, 2000;
accepted July 31, 2000.)